10-6-2003

Tomographic reconstruction of treponemal cytoplasmic filaments reveals novel bridging and anchoring components

Jacques Izard

Bruce F. McEwen

Rita M. Barnard

Thomas Portuese

William A. Samsonoff

See next page for additional authors

Authors

Jacques Izard, Bruce F. McEwen, Rita M. Barnard, Thomas Portuese, William A. Samsonoff, and Ronald J. Limberger

Molecular Microbiology (2004) **51**(3), 609–618 doi:10.1046/j.1365-2958.2003.03864.x

Tomographic reconstruction of treponemal cytoplasmic filaments reveals novel bridging and anchoring components

Jacques Izard,[1,3]* Bruce F. McEwen,[2,3] Rita M. Barnard,[2] Thomas Portuese,[2] William A. Samsonoff[2] and Ronald J. Limberger[1,3]

[1]*New York State Department of Health, Wadsworth Center, David Axelrod Institute for Public Health, PO Box 22002, Albany, New York 12201–2002, USA.*

[2]*New York State Department of Health, Wadsworth Center, Biggs Laboratory, PO Box 509, Albany, New York 12201–0509, USA.*

[3]*Department of Biomedical Sciences, State University of New York at Albany, Albany, New York 12201, USA.*

Summary

An understanding of the involvement of bacterial cytoplasmic filaments in cell division requires the elucidation of the structural organization of those filamentous structures. Treponemal cytoplasmic filaments are composed of one protein, CfpA, and have been demonstrated to be involved in cell division. In this study, we used electron tomography to show that the filaments are part of a complex with a novel molecular organization that includes at least two distinct features decorating the filaments. One set of components appears to anchor the filaments to the cytoplasmic membrane. The other set of components appears to bridge the cytoplasmic filaments on the cytoplasmic side, and to be involved in the interfilament spacing within the cell. The filaments occupy between 3 and 18% of the inner surface of the cytoplasmic membrane. These results reveal a novel filamentous molecular organization of independent filaments linked by bridges and continuously anchored to the membrane.

Introduction

Treponema species are the aetiologic agents of several diseases including syphilis (Woltsche-Kahr *et al*., 1999; Collighan *et al*., 2000; Wicher *et al*., 2000; Asai *et al*., 2002; Paster *et al*., 2002). Some species are involved in the progression and severity of periodontal disease, which affects millions of people (Armitage *et al*., 1982; Moter *et al*., 1998; Simonson *et al*., 1988; Paster *et al*., 2001). Those species involved in the progression of periodontal disease have also recently been detected in atherosclerotic lesions (Okuda *et al*., 2001), and in the brains of Alzheimer's disease patients (Riviere *et al*., 2002). Although treponemes may not be the aetiologic agents of those diseases, their detection underscores their ability to overcome the protective barriers of the human body, as suggested by *in vitro* experiments (Thomas *et al*., 1988; Brissette and Lukehart, 2002).

A filamentous ribbon-like structure composed of a minimum of two to six filaments is present in the cytoplasm of all treponemal cells (Hovind-Hougen, 1976; Holt, 1978; Izard *et al*., 1999). The presence of cytoplasmic filaments has been documented, by electron microscopy, in *Treponema*, *Leptonema*, *Spirochaeta*, *Pillotina*, *Hollandina* and *Diplocalyx* species (Hollande *et al*., 1967; Holt, 1978; Hovind-Hougen, 1979; Bermudes *et al*., 1987; Bermudes *et al*., 1988). The cytoplasmic filaments are located underneath the periplasmic flagellar bundle, in close apposition to the cytoplasmic membrane (Hovind-Hougen, 1974; Eipert and Black, 1979). The individual filaments maintain a ribbon-like configuration (Eipert and Black, 1979; Izard *et al*., 1999), and the periodicity of the helix of the bundle is equivalent to the cell's helical periodicity (Zemper and Black, 1978). The cytoplasmic filaments span the length of the treponemal cell, and are not a transitory structure (Izard *et al*., 1999); they are found in cells at all growth stages. The filaments are severed during cell division, so that roughly half of the length of the bundle remains in each daughter cell (Eipert and Black, 1979; Izard *et al*., 1999). We chose *Treponema phagedenis* as a model for electron microscopic work because of the relatively high contrast of the cytoplasmic filament, and their relatively high number, compared to other species (Izard *et al*., 1999).

The treponemal cytoplasmic filaments are composed of a unique 82 kDa protein, CfpA (Masuda and Kawata, 1989; You *et al*., 1996; Izard *et al*., 1999). There is no sequence similarity between CfpA and other known or

Accepted 6 October, 2003. *For correspondence at New York State Department of Health, Wadsworth Center, David Axelrod Institute for Public Health, PO Box #22002, 120 New Scotland Avenue, Albany, New York 12201–2002, USA. E-mail izard@wadsworth.org; Tel. (+1) 518 474 4177; Fax (+1) 518 486 7971.

predicted open reading frame products. The amino acid sequence is well conserved among species of *Treponema* (Izard *et al*., 1999), and the proteins share common antigens (Masuda and Kawata, 1989; You *et al*., 1996).

We have recently used gene interruption to abolish the expression of *cfpA* in *T. denticola* (Izard *et al*., 2001). The severe pleiotropic defects that were observed included formation of chains of cells (filamentation), production of anucleate cells (DNA-less cell), and in contrast to the wild-type bacteria, a highly condensed chromosomal DNA. A much less stringent but similar pleiotropic cell division defect has been observed in a *recA* minus mutant of another spirochete, *Leptospira biflexa* (Tchamedeu Kameni *et al*., 2002). The *cfpA* knockout-mutant phenotypes suggest that the cytoplasmic filaments are involved in chromosome structure, segregation, and/or in the cell division process, in treponemal cells (Izard *et al*., 2001).

Electron tomography has recently emerged as a powerful tool for three-dimensional (3D) imaging of biological machines in their native contexts (Grimm *et al*., 1998; McEwen and Marko, 2001; Baumeister, 2002). As in medical applications of tomography, a 3D volume is reconstructed from a series of two-dimensional (2D) images recorded at various viewing angles (Crowther *et al*., 1970; McEwen and Marko, 1999). The advantage of this approach is that it can be used to obtain a complete 3D reconstruction of complex and irregularly shaped structures at moderately high resolutions.

Recent applications include the detection of conformational changes of the myosin cross-bridges in insect flight muscle (Taylor *et al*., 1999); a study of the gamma-tubulin ring complex, leading to an explicit molecular model for template initiation of microtubule assembly (Moritz *et al*., 2000); and the deduction of subunit arrangements in fibrillin-rich microfibrils (Baldock *et al*., 2001). *In situ* applications include finding novel information about early mitotic spindle arrangement in *Saccharomyces cerevisiae* (O'Toole *et al*., 1999); the detection of component parts in frozen-hydrated axonemes (McEwen *et al*., 2002); and the visualization of the actin cytoskeleton in frozen-hydrated preparations of *Dictyostelium* (Medalia *et al*., 2002). These and several other studies have demonstrated the utility of electron tomography in determining the arrangement and location of macromolecular attachments on fibrous structures.

In the current study, we present the first application of electron tomography to bacterial cytoplasmic filaments *in situ*, and the first high-resolution tomographic reconstruction of a bacterial protein complex *in situ*. The tomographic reconstructions that we obtained provide a 3D mapping of the cytoplasmic filaments in *Treponema phagedenis*, as well as information about decorating features of the filaments. This map enabled us to confirm the overall helical course of the filament bands, and to develop a new model in which the cytoplasmic filaments are part of a 'cytoskeleton-like' protein complex, with a molecular organization composed of independent filaments linked by bridges and continuously anchored to the membrane.

Results

Treponema bacteria have an inner and outer cell membrane delimiting a periplasm in which the flagellar filaments are located. The outer membrane must be removed to free the flagella in order to observe the low-contrast cytoplasmic filaments located beneath the flagellar bundle (Fig. 1) (Hovind-Hougen and Birch-Andersen, 1971; Hovind-Hougen, 1972; 1974; Izard *et al*., 1999). The water-based treatment has been proven to be the most consistent way to prepare cells for observation. Although chemical treatments by detergent are quicker, the resulting level of structural preservation is insufficient for tracking the cytoplasmic filaments, or for observing the cell ends (J. Izard and W. A. Samsonoff, unpubl. obs.).

Traditional 2D electron microscopic analysis has a limited capacity for deciphering spatial relationships between the cytoplasmic filaments. Therefore, electron tomography was used to obtain a more accurate analysis of the sizes and arrangement of the cytoplasmic filaments and asso-

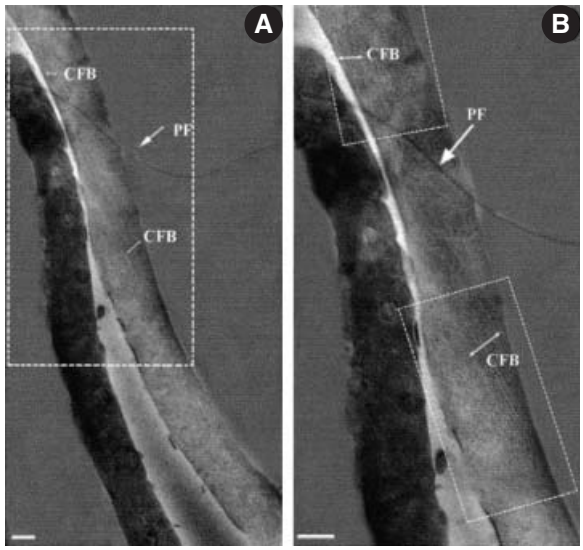

Fig. 1. Zero degree tilt image from a tomographic series of a negatively stained *T. phagedenis* cell.
A. Overview of the full image. Note that the outer membrane of the neighbouring left cell has been only partially removed. This image was digitally modified to balance greyscale levels between the cell and the background.
B. Higher-magnification view of the area outlined by the dashed-line box in A. Note the well-formed band of cytoplasmic filaments. The dashed boxes in the lower right and upper left roughly correspond to areas examined in greater detail by electron tomography in Figs 2 and 6. PF – periplasmic flagellum; CFB – cytoplasmic filament band. Scale bars = 100 nm.

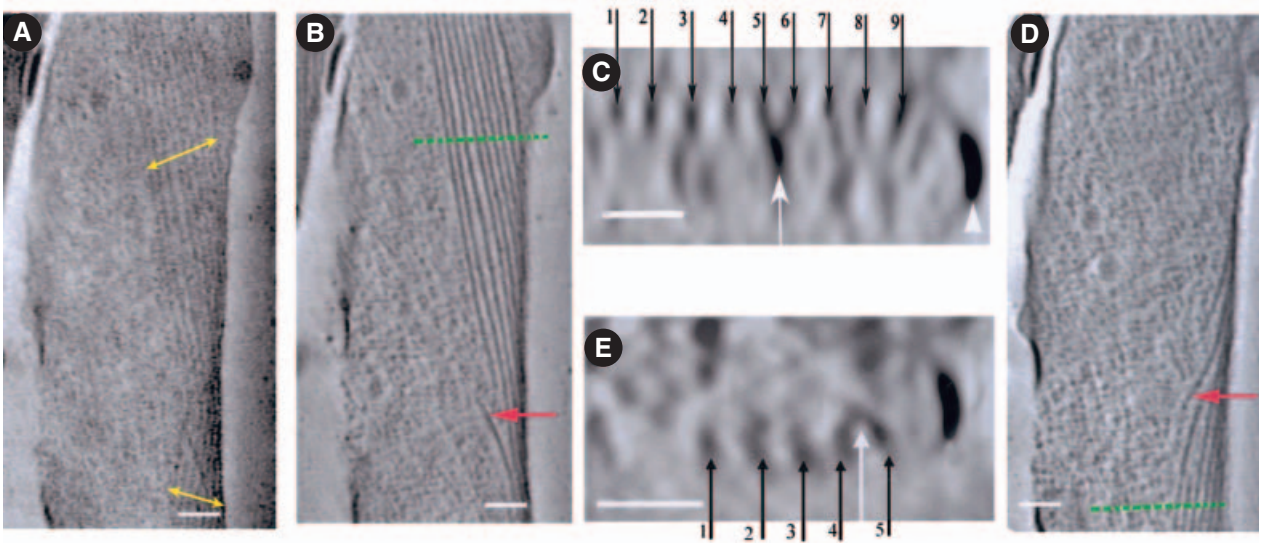

Fig. 2. Tomographic reconstruction of a negatively stained *T. phagedenis* wild-type cell.
A. The zero-degree image from a tomographic tilt series that includes the section shown in the lower right dashed box shown in Fig. 1B. Yellow arrows indicate two bands of nine cytoplasmic filaments that emerge from the cell cylinder edge. Although the bands appear to be part of a single filament band that undergoes a twist at the cell wall, this cannot be definitively determined from a single 2D image.
B. A 2 nm-thick planar slice from the tomographic 3D reconstruction. This slice is taken from a depth that is roughly at the centre of the upper band of filaments in A. Red arrow indicates an apparent break in one of the filaments. The filaments in the lower band can be seen in planar slices taken from a different depth in the 3D reconstruction (see D).
C. A 2 nm-thick axial slice showing the filament cross-sections (black arrows). This slice is taken from the level indicated by the dashed green line in B. The white arrow indicates a structure bridging two filaments whereas the white arrowhead indicates remnants of the cell wall, or stain accumulation.
D. A 2 nm-thick planar slice through the band of filaments on the other side of the turn of the filament band, as indicated by the bottom yellow arrow in A. Red arrow indicates the end of an apparently broken filament.
E. A 2-nm axial slice through the level indicated by the dashed green line in D. As in C, the black arrows indicate five filament cross-sections and the white arrow indicates a bridging structure. The other four filaments emerge at a lower position from the turn. Scale bars for A, B and D = 50 nm. Scale bars for C and E = 25 nm.

ciated features. Figure 2 shows a 3D reconstruction of a *T. phagedenis* cell from a tilt series of images recorded at a 1.5° angular interval over a range of −57.0 to +58.5°. A single 2 nm thick slice through the reconstruction is shown in Fig. 2B. The filaments appear much more sharply defined than in the zero-degree projection image (Fig. 2A), because they have been imaged at a single level in the cell, without interference from material above and below the band. The other band of filaments indicated in Fig. 2A becomes visible at a different depth in the cell with little trace of the filaments in the intervening levels (Figs 2D and 3B; see also the movie through the volume

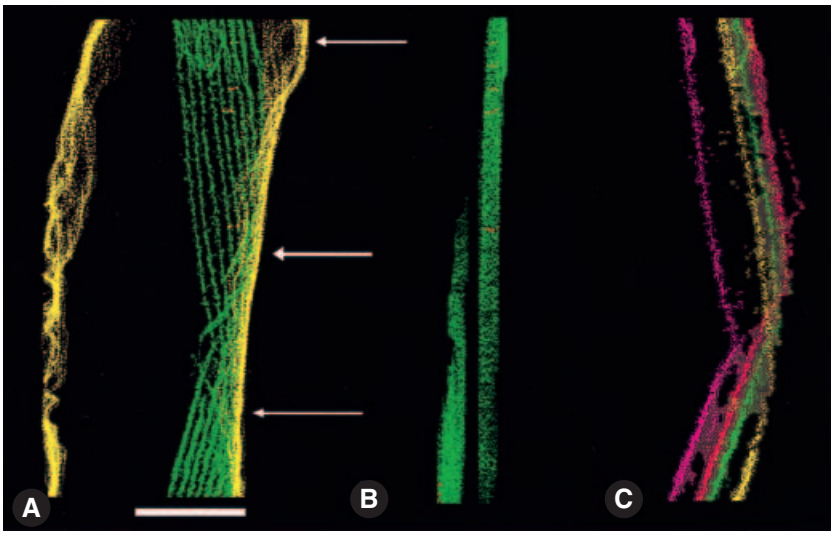

Fig. 3. 3D model of cytoplasmic filaments in a negatively stained cell traced from planar views such as those shown in Fig. 2B and D.
A. The model is oriented as in Fig. 2A with the filaments shown in green and the unidentified electron dense material in yellow. Note the broken filaments and a slight skewing between the orientations of the two filament bands.
B. As in A, but with the model viewed from the side (viewing direction indicated by the white arrows in A). The visualization of the electron dense material (yellow) has been turned off in this display. The different depths of the two filament bands are evident in this view.
C. Colour-coding to indicate four pairs of filaments, one from each band, whose ends align in the model. The filaments have been coloured independently to show their individual continuity. Model orientation is as in A. Scale bar = 100 nm.

in *Supplementary material*). Figure 2C and E show cross-sectional views of the filament bands in axial slices taken from the areas indicated by the dashed green lines in Fig. 2B and D). Connections between the filaments can be detected in these views (white arrows). The whole cell has an elliptical cross-section with a reduced depth dimension indicating that the cell is flattened during the negative stain preparation. The shearing forces of the collapse during drying may have given rise to the broken filaments seen in Figs 2B and D, and Fig 3A.

The filaments and the electron-dense material, which may represent peptidoglycan, membrane, associated protein and negative stain build up along the sides of the cell (the unidentified electron-dense material is coloured yellow in Fig. 3A), were traced from planar views such as Fig. 2B and D, and Fig. 3A–C. Examination of the 3D reconstruction reveals that the two bands of filaments indicated in Fig. 2A are located on the upper and lower surfaces of the tomographic reconstruction, and are separated by an intervening gap (Fig. 3B). Nevertheless, the ends of individual filaments from the two bands align which indicates that they are part of the same filament band (Fig. 3C). Similar analyses from two other cells confirmed these results.

From the 3D volume, we could make accurate measurements of the size and spacing of individual cytoplasmic filaments. However, the vertical measurement must be corrected for an elongation that occurs in the Z direction as a result of the limited tilt range (Frank and Radermacher, 1986). For a $\pm 60^\circ$ tilt range the elongation factor is 1.55. Applying this correction, we find the fibre dimensions to be $5.0 \pm 0.5 \times 6.0 \pm 0.5$ nm (horizontal/vertical or width/depth) in cross-section, with an average interfilaments spacing of 10.4 ± 1.8 nm. The filaments are independent of each other. No direct filament-to-filament contacts were detected in the absence of breakage.

The 3D reconstructions also enabled us to detect cross-bridges between individual filaments of the band (Fig. 2C,E). These connections form arch-like structures that protrude above the filament band on its cytoplasmic side. Because these connections are largely located at a different depth than the filaments, we can only detect them in axial views (cross-section) of the filament band. Although this is a lower resolution direction, the cross-bridges are large enough to be clearly discerned. We created 3D models of the cross-bridge network over a selected area of the filament band by tracing the filaments and cross-bridges in axial views (e.g. Fig. 2C and E). The results are shown in Fig. 4 with filaments colour–coded in green and cross-bridges in red. The network of cross-links appears collapsed and irregular in these views. Analysis of the two other cells confirmed these results.

On the opposite side of the filaments, we detected structures that apparently connect the filaments to the inner side of the cytoplasmic membrane. In contrast to the cross-bridges on the cytoplasmic side of the filament band, connectors on the membrane side are more elongate, rarely form cross-bridges between filaments, and appear to be more densely packed along the filament axis (Fig. 5).

We computed a tomographic reconstruction from the upper portion of the cell shown in Fig. 1B. This reconstruction contains the ends of five of the cytoplasmic filaments in the band (Fig. 6). A tomographic reconstruction from the adjacent region contained the ends of the other four filaments (data not shown). Careful examination of this reconstruction reveals that individual cytoplasmic filaments in the band terminate randomly with no apparent connection to the inner-membrane associated flagellar basal-body, or to any other definable structure within the cytoplasm (Fig. 6). All of the above features were also

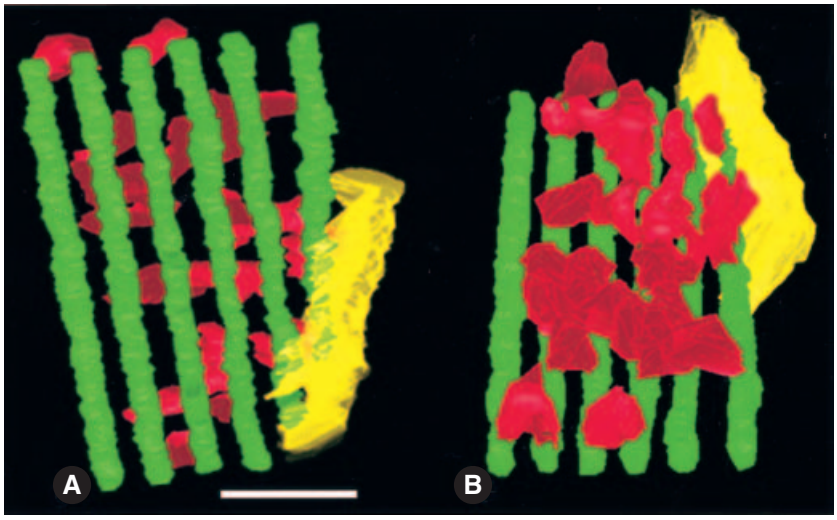

Fig. 4. 3D model of cytoplasmic filaments and filament bridging structures. The model was traced from axial views such as those in Fig. 2C and E. For simplicity, six of the nine filaments from the upper band in Fig. 2A–C were traced over a limited distance. Filaments are shown in green, the unidentified electron dense material in yellow, and apparent interfilament connections in red.
A. Model viewed from approximately the same orientation as in Figs 2A and 3A (view from the periplasmic side).
B. Model viewed from the opposite side (cytoplasmic side). Note that the connections form an irregular lattice on one side of the filament band. Scale bar = 25 nm.

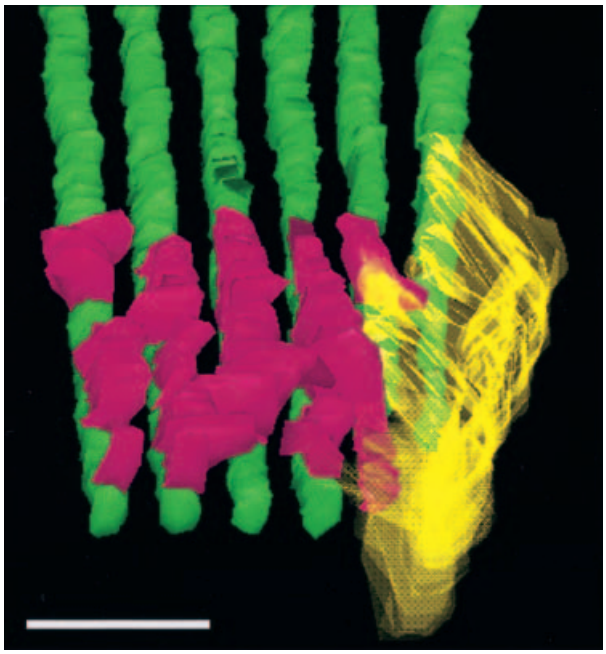

Fig. 5. Apparent membrane connections on cytoplasmic filaments. The same model as shown in Fig. 4, rotated to illustrate filament connections that are on the opposite side of the filaments. Filaments are shown in green, the unidentified electron dense material in yellow, and the membrane connections in magenta. The model is viewed from the same side of the filament band as in Figs 2A, 3A and 4A (periplasmic side), but at a more oblique angle to highlight the distribution of the putative membrane connectors. For clarity, the connectors, which form an almost continuous 'curtain' on the membrane side of the filaments, have been only drawn on the lower portion of the figure. Scale bar = 25 nm.

detected in tomographic reconstructions from the two other cells.

Discussion

In this study, we have used electron tomography to elucidate 3D relationships between individual cytoplasmic filaments and other cellular elements at high resolution. This approach avoids artifacts of 2D analysis and provides new insights on the protein complexes involved in the formation and function of the cytoplasmic filament bands.

The effects of specimen preparation are always a concern for structural analysis. Cytoplasmic filaments cannot be observed by negative staining in *Treponema*, unless the outer membrane is removed to release the flagella. Experience has shown that the most efficient way to remove the outer membrane is by hypotonic treatment. Chemical (detergents) or enzymatic (lipase) treatments either only partially strip the outer membrane, or destroy important cellular structures (J. Izard and A. Samsonoff, unpubl. data). Although milder than the alternatives, hypotonic extraction does introduce the possibility that the irregular distribution of cross-bridges on the cytoplasmic side of the filaments arises because protein complexes have been dissociated, or degraded by cell proteases. However, because the density of the bridging structures is high, we cannot exclude the possibility of a continuous structure decorating the filaments on the cytoplasmic side as it appears on the periplasmic side.

We tracked the course of one cytoplasmic filament band over two full turns in the cell, and observed that the band alternately lies on the upper part and the lower part of the

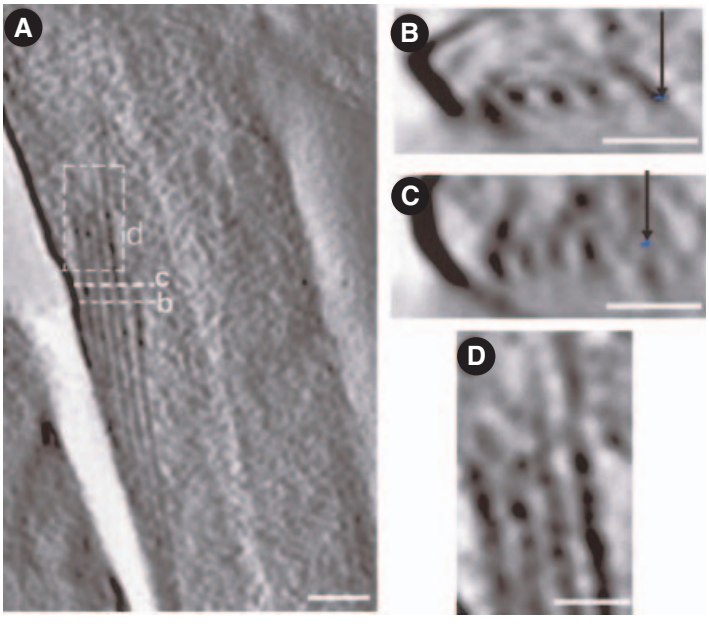

Fig. 6. Termination sites of cytoplasmic filaments at the cell end.
A. A 2 nm-thick planar slice through a tomographic reconstruction from the upper left region of the cell in Fig. 1B. This slice contains the ends of five of the cytoplasmic filaments from the band illustrated in Figs 2–5. Dashed lines and a dashed box indicate the locations of higher magnification views in B–D.
B. Axial view taken from the level indicated in A. Cytoplasmic filaments have a similar cross-sectional view to those seen in Fig. 2. The arrow points to the blue spot that indicates the cross-section of the filament in the far right side of the band just before the filament terminates.
C. Same view as B, taken slightly further down the filament band as indicated in A. This location is just past the end of the far right filament whose approximate location is marked by the blue spot, indicated by the arrow. No end-connecting structures were apparent in this view, in B, or in any of the intervening views.
D. Planar view of the area indicated by the dashed box in A. This view includes the ends of three of the filaments. Again, no notable structures were located at the filament ends.
Scale bar = 50 nm in A, 25 nm in B–D.

cytoplasmic cylinder, with the changeover occurring during turns at the sides of the cell (Figs 2 and 3). Although there is an apparent gap in the filament band at the changeover points (Fig. 3B), the number of filaments in the band is conserved through the turns and we were able to roughly align individual filaments from the two levels (Fig. 3C). These results indicate that the filament band is a continuous structure that follows a helical path along the long axis of the cell just beneath the cytoplasmic membrane. During specimen preparation by negative staining, there is a build up of negative stain at the sides of the cell. The filament contrast is lost in the dense stain buildup and the filament bands appear to be discontinuous. Thus, our data confirm previous deductions made from two-dimensional electron microscopy that the filaments form a continuous band following a helical path along the long axis of the cell (Izard *et al.*, 1999).

From the computed 3D tomographic reconstruction, we were able to accurately determine the dimensions of the cytoplasmic filaments. After correction for the computational elongation, we obtain an average cross-sectional dimension of 5.0×6.0 nm $\pm$ 0.5 nm for an individual cytoplasmic filament. Given the uncertainty due to vertical distortion and the limiting resolution of 5–6 nm, we conclude that the fibre is at most only slightly elliptical in cross-section.

Previously, in *T. pallidum*, the horizontal cross-section of cytoplasmic filaments was estimated to be 7–7.5 nm as determined by 2D electron microscopy (You *et al.*, 1996). Their measurements represent roughly the half of the length of two filament sections and their in-between gap, as determined by our experiments. The interfilament space was not included in their measurement because the 2D images suggested that adjacent filaments are tightly packed with no significant interfilament space. Similar results were observed in *T. refringens* and *T. reiter* (Hovind-Hougen and Birch-Andersen, 1971; Eipert and Black, 1979). Slightly wider filaments (about 9 nm wide) were described in *Treponema* sp. strain E-21 and *T. pertenue* (Jackson and Black, 1971; Masuda and Kawata, 1989). Our measurement of the filaments cross-section represents a refined measurement of the structure. Moreover, our 3D reconstruction eliminates the artifact of 2D observation leading to conclude that the filaments are tightly packed with interfacing surfaces between the filaments.

Previous estimates of the vertical cross-section vary widely. These range from about 1 nm for *T. pallidum* filaments (You *et al.*, 1996), to 3 nm for *Treponema* sp. strain E-21 filaments (Masuda and Kawata, 1989), to 7.5 nm (as diameter of a tubular structure) for *T. reiter* filaments (Hovind-Hougen and Birch-Andersen, 1971; Masuda and Kawata, 1989). The difficulties in resolving the filament thickness are due to the predicted shape of the filaments and their close association with the cytoplasmic membrane, both *in situ* and in purified filaments. Cross-sections of the cytoplasmic filaments were reported to be wedge- or comma-shaped (Swain and Anderson, 1972), tubular (Jackson and Black, 1971), or oblong (Wiegand *et al.*, 1972). Moreover, the associated membrane may have interfered with filament staining and thereby hindered the ability to decipher distances. Observation of the cross-section of the filament using the tomographic data allowed the definition of two characteristics: the slight elliptical nature of the filaments with a defined boundary distinct from the background on all sides, and distant of the adjacent filament in the band. These observations allowed further investigation of the characteristics of the filament organization.

Electron tomography has also enabled us to uncover several novel features of the cytoplasmic filament organization. First, the filaments are independent of each other with no direct filament-to-filament contact. Second, there are cross-bridging structures between neighbouring filaments. These cross-bridges are located on the cytoplasmic side of the filament band where they maintain the distance between individual filaments; they probably function to maintain structural solidarity of the band and they likely interact with other cytoplasmic components. Third, there are proteins attached to the periplasmic side of the filament band that are associated with the cytoplasmic membrane and presumably function to anchor the band.

The centre-to-centre spacing between individual filaments is 10.4 nm $\pm$ 1.8 nm. The large standard deviation for the spacing measurement indicates that there is some variability in the distance between the filaments, even though long stretches of ribbon have been observed with nearly uniform spacing. Such a variation in distance between the filaments could arise from the loss of connecting bridges during specimen preparation, allowing a greater flexibility in the organization of filaments.

Overall, three to 10 cytoplasmic filaments were observed per cell in *T. phagedenis*, with a mean of 5.7 (Izard *et al.*, 1999). Based on the centre-to-centre spacing of the filaments, the horizontal cross-section of the filaments, and an estimated diameter of the cytoplasmic cylinder of 200 nm, we estimate that the cytoplasmic filament band covers between 3 and 18% (average, 7–9%) of the cross-section of the inner surface of the cytoplasmic membrane. The standard deviations of the measurements were used in calculating the percentages for lowest and highest values. The surface association of the cytoplasmic filament structure with the inner side of the cytoplasmic membrane is significant. Although abolition of the cytoplasmic filament gene expression is not lethal, cell growth, motility and cell division are directly affected by the absence of such filaments, underlining the physiological

importance of this anchored filamentous structure (Izard *et al*., 2001).

The nature of the protein that associates the cytoplasmic filaments with the inner side of the cytoplasmic membrane is unknown. The membrane connectors vary in length from 8.5 to 13.5 nm, whereas their width is approximately the same as the filaments. Previous experiments, based on 2D electron micrographs of freeze-etched *T. refringens* cells, show that a filamenteous structure deforms the cytoplasmic membrane and leaves an impression (Eipert and Black, 1979). The thickness of a bacterial membrane is between 7 and 9 nm (Gennis, 1989). Thus, it is possible that the anchoring protein is an integral inner-membrane protein or a lipoprotein that functions to anchor the filaments to the membrane.

In agreement with previous reports (Hovind-Hougen, 1976; Izard *et al*., 1999), we find no progressive decrease in the filament numbers over the last helical turn of the cell. Rather, the filament band ends abruptly near the ends of the cell (Fig. 6). We found no indication that cytoplasmic filaments are connected to the inner-membrane associated flagellar basal body, thus, this observation by Hovind-Hougen and Birch-Andersen (1971) remains unconfirmed. Previously we observed two instances where filament ends were associated with a membranous structure, suggesting that there is a unique anchor for filaments associated with the membrane at the cell end (Izard *et al*., 1999). We were not able to find this type of cell structure in the cells used for tomographic analysis. Thus, electron tomography indicates that either the filaments end close to the cell ends, attached solely by the anchor proteins in the membrane, or that the filaments break off their putative anchor at the cell tip, and the filaments regain their regular spacing close to the suspected breakage point (Fig. 6).

Cryo-electron microscopy of vitrified cells has the potential to alleviate limitations as a result of structural alterations during specimen preparation (McEwen *et al*., 2002; Medalia *et al*., 2002). This technology enables visualization of fully hydrated, vitreous specimens prepared by rapid freezing. Such specimens exhibit minimum structural alterations or cellular collapse. The recent analysis of a Dictyoselium cell opens a new horizon in imaging cellular structure in the native state (Medalia *et al*., 2002). Nevertheless, the Dictyostelium study was limited to analysis of the thin edge of the cell periphery. In contrast spirochetes and other prokaryotes are small enough for whole cell imaging at low resolution (Grimm *et al*., 1998). Although application of cryo-electron tomography to *Treponema* cells could be straightforward, because of the high density of the cytoplasm, and the presence of periplasmic flagella covering part or all of the cytoplasmic filament band, the removal of the outer-membrane is still required so that the cytoplasmic filaments have sufficient contrast for visualization.

The observation of cytoskeletal assemblies in prokaryotes raises the issue of sequence similarity between prokaryotic and eukaryotic cytoskeleton proteins (Jenkins *et al*., 2002). Prokaryotic filamentous structures that are either involved or hypothesized to be involved in cell division include FtsA, FtsZ, CafA and some as-yet uncharacterized structures (Eipert and Black, 1979; Bi and Lutkenhaus, 1991; Gayda *et al*., 1992; Bermudes *et al*., 1994; Okada *et al*., 1994; You *et al*., 1996). FtsA and FtsZ are essential for cell septation (Bi and Lutkenhaus, 1991; Addinall and Lutkenhaus, 1996; Ma *et al*., 1996; Wang *et al*., 1997) and are related, respectively, to actin and tubulin (Sanchez *et al*., 1994; Erickson *et al*., 1996). MreB (an actin homologue) forms cytoplasmic filament structures involved in cell-shape control in *Bacillus subtilis* (Jones *et al*., 2001), and is also present in *T. pallidum* (Fraser *et al*., 1998). Other cytoplasmic filament structures such as microtubules, tubules, fibres, fibrils and filaments have been described in prokaryotes, but their function is unknown (Bermudes *et al*., 1994).

In *T. denticola*, the permanence of the cytoplasmic filaments at all stages of cell division and growth, their organization in ribbon form, and the apparent absence of an effect on cell structure in a *cfpA* minus mutant, differentiate these filament structures from the filaments observed in *E. coli* and *B. subtilis*. Nevertheless, the *cfpA* minus mutant phenotype does indicate a critical role for the cytoplasmic filaments in cell division, chromosome condensation, and/or chromosome segregation. Therefore, continued study of this persistent structure will bring critical new insights on several key cellular functions, and will improve our understanding of the mechanisms involved in transient or permanent structures in other bacteria.

Experimental procedures

Strains, reagents, culture and molecular methods

Treponema phagedenis Kazan 5 (Limberger and Charon, 1986) was grown in Spirolate broth (Becton Dickinson Microbiology Systems, Cockeysville, MD) with 10% heat-inactivated rabbit serum, in an anaerobic chamber (Coy Laboratory Products, Grass Lake, MI) under an atmosphere of 85% nitrogen, 10% hydrogen and 5% carbon dioxide.

To prepare cells for electron microscopy, 2 ml of an early exponential phase growth culture of wild-type *T. phagedenis* were centrifuged for 1 min at 10 000 *g*. The cells were re-suspended in the same volume of sterile distilled water and stored at 4°C overnight, centrifuged, and re-suspended in 100 μl of sterile distilled water before use.

Electron microscopy and electron tomography

Cell suspensions were applied to a Formvar support film on 200-mesh grids and were negatively stained with 2% sodium phosphotungstate (pH 7.0) as previously described (Izard

et al., 1999). Stained specimens were imaged at 25,000 × or 31,500 × magnification in a Zeiss (LEO) 910 transmission electron microscope operating at 120 KeV. All images were recorded on SO 163 electron image film (Kodak, Rochester, NY), and the film was developed according to standard procedures. The defocus was approximately of 1.5 microns. The total electron dose is approximately of 40 000 electrons per $(nm)^2$.

Electron tomographic tilt series were collected for six individual cells, and 3D reconstructions were computed for three of these cells. Cells were selected for data collection according to the criteria that the cytoplasmic filaments be visible in the untilted view; that the long axis of the cell be approximately aligned with the tilt axis of the electron microscope's goniometer; and that the cell be near the centre of the specimen grid to minimize occlusion by the standard LEO specimen holder at high tilt angle. Tilt images were collected at a 1.5° angular interval over a ±60° angular range. At high tilt angles, the cells tended to be 'overshadowed' by the relatively large buildup of negative stain at the sides of the cells. This technical limitation was overcome by collecting the tilt series at a higher magnification than required for electron tomography, and by giving extra exposure to higher-tilt images. Image intensities were roughly balanced in the subsequent digitization step.

Tilt series images were digitized with a pixel size of 0.78 nm and aligned using small features of the field as fiduciary markers (Landis *et al*., 1993). Tomographic 3D reconstructions were computed as described by McEwen and Marko (1999). Assuming that *T. phagedenis* cells are roughly cylindrical, with a diameter of 200 nm, the resolution of the 3D reconstruction is limited by the angular sampling to 5–6 nm in the X-Y direction and 8–9 nm in the Z direction (Crowther *et al*., 1970; McEwen *et al*., 2002). Cytoplasmic filaments, filament cross-bridges, and membrane connectors were segmented from the reconstruction volume by manual tracing using the IMOD software package (Kremer *et al*., 1996). The 'XYZ' utility in IMOD greatly improves the accuracy of manual tracing, because it enables the operator to monitor the cursor position from three orthogonal viewing directions while tracing. All other operations were performed with commands in the SPIDER software package (Frank *et al*., 1996). Cytoplasmic filaments were traced lengthwise from planar slices (Fig. 3), or axially from axial slices for display (Figs 4 and 5). The latter orientation was required for the identification of bridging structures and membrane connectors. Traced contours were stacked and filled using the appropriated IMOD utilities. Figures were constructed and edited in Photoshop 5.5 (Adobe Systems, San Jose, CA).

IMOD was used to measure cytoplasmic filament dimensions and interfilament spacings from 25 different cross-sectional slices (X-Z slices) of the tomographic reconstructions from all three cells. The slices were digitally magnified by four to increase accuracy. Distances were measured in pixels and surface locations were verified using the 'XYZ' utility. For calculation of the vertical and horizontal dimensions of the fibre, one pixel was added to the measurements to compensate for edge effects. All measurements were then divided by four and multiplied by the pixel size (0.78 nm) to convert pixel lengths to nanometres.

Acknowledgements

This work was supported by the National Institutes of Health (NIH) Public Health Service grant AI34354, and the NIH-NCRR grant P41 RR01219 that supports the Wadsworth Center's Resource for Biological Complexity as a National Biotechnological Resource. We also thank the Wadsworth Center's Core Facility for Electron Microscopy.

Supplementary material

The following material is available from
http://www.blackwellpublishing.com/products/journals/suppmat/mmi/mmi3864/mmi3864sm.htm

Fig. S1. Movie through the planes parallel to the cytoplasmic filaments of the 3D reconstruction of the *T. phagedenis* cell presented in Figs 2 and 3. The decorating features of the filaments are not obvious because of their orientation.

References

Addinall, S.G., and Lutkenhaus, J. (1996) FtsA is localized to the septum in an FtsZ-dependent manner. *J Bacteriol* **178:** 7167–7172.

Armitage, G.C., Dickinson, W.R., Jenderseck, R.S., Levine, S.M., and Chambers, D.W. (1982) Relationship between the percentage of subgingival spirochetes and the severity of periodontal disease. *J Periodontol* **53:** 550–556.

Asai, Y., Jinno, T., Igarashi, H., Ohyama, Y., and Ogawa, T. (2002) Detection and quantification of oral treponemes in subgingival plaque by real-time PCR. *J Clin Microbiol* **40:** 3334–3340.

Baldock, C., Koster, A.J., Ziese, U., Rock, M.J., Sherratt, M.J., Kadler, K.E., *et al.* (2001) The supramolecular organization of fibrillin-rich microfibrils. *J Cell Biol* **152:** 1045–1056.

Baumeister, W. (2002) Electron tomography: towards visualizing the molecular organization of the cytoplasm. *Curr Opin Struct Biol* **12:** 679–684.

Bermudes, D., Chase, D., and Margulis, L. (1988) Morphology as a basis for taxonomy of large spirochetes symbiotic in wood-eating cockroaches and termites: *pillotina* gen nov., nom. rev., *Pillotina calotermitidis* sp. nov., nom. rev., *Diplocalyx* gen nov., nom. rev., *Diplocalyx calotermitidis* sp. nov., nom. rev., *Hollandina* gen nov., nom. rev., *Hollandina pterotermitidis* sp. nov., nom. rev. & *Clevelandina reticulitermitidis* gen nov., sp. nov. *Int J Syst Bacteriol* **38:** 291–302.

Bermudes, D., Fracek, S.P. Jr, Laursen, R.A., Margulis, L., Obar, R., and Tzertzinis, G. (1987) Tubulinlike protein from *Spirochaeta bajacaliforniensis*. *Ann N Y Acad Sci* **503:** 515–527.

Bermudes, D., Hinkle, G., and Margulis, L. (1994) Do prokaryotes contain microtubules? *Microbiol Rev* **58:** 387–400.

Bi, E.F., and Lutkenhaus, J. (1991) FtsZ ring structure associated with division in *Escherichia coli*. *Nature* **354:** 161–164.

Brissette, C.A., and Lukehart, S.A. (2002) *Treponema denticola* is resistant to human beta-defensins. *Infect Immun* **70:** 3982–3984.

Collighan, R.J., Naylor, R.D., Martin, P.K., Cooley, B.A., Buller, N., and Woodward, M.J. (2000) A spirochete isolated from a case of severe virulent ovine foot disease is closely related to a Treponeme isolated from human periodontitis and bovine digital dermatitis. *Vet Microbiol* **74:** 249–257.

Crowther, R.A., De Rosier, D.J., and Klug, A. (1970) The reconstruction of a three-dimesional structure from the projections and its application to electron microscopy. *Proc R Soc London* **A317:** 319–340.

Eipert, S.R., and Black, S.H. (1979) Characterization of the cytoplasmic fibrils of *Treponema refringens* (Nichols). *Arch Microbiol* **120:** 205–214.

Erickson, H.P., Taylor, D.W., Taylor, K.A., and Bramhill, D. (1996) Bacterial cell division protein FtsZ assembles into protofilament sheets and minirings, structural homologs of tubulin polymers. *Proc Natl Acad Sci USA* **93:** 519–523.

Frank, J., and Radermacher, M. (1986) Three-dimensional reconstruction of non-periodic macromolecular assemblies from electron micrographs. In *Advanced Techniques in Biological Electron Microscopy III*, **Vol. 3**. Koehler, J.K., (ed). Berlin: Springer-Verlag, pp. 1–72.

Frank, J., Radermacher, M., Penczek, P., Zhu, J., Li, Y., Ladjadj, M., and Leith, A. (1996) SPIDER and WEB: processing and visualization of images in 3D electron microscopy and related fields. *J Struct Biol* **116:** 190–199.

Fraser, C.M., Norris, S.J., Weinstock, G.M., White, O., Sutton, G.G., Dodson, R., *et al.* (1998) Complete genome sequence of *Treponema pallidum*, the syphilis spirochete. *Science* **281:** 375–388.

Gayda, R.C., Henk, M.C., and Leong, D. (1992) C-shaped cells caused by expression of an *ftsA* mutation in *Escherichia coli*. *J Bacteriol* **174:** 5362–5370.

Gennis, R.B. (1989) *Biomembranes: Molecular Structure and Function*. New York: Springer-Verlag.

Grimm, R., Singh, H., Rachel, R., Typke, D., Zillig, W., and Baumeister, W. (1998) Electron tomography of ice-embedded prokaryotic cells. *Biophys J* **74:** 1031–1042.

Hollande, A., Gharagozlou, I., and Grasse, P. (1967) Morphologie infrastructurale de *Pillotina calotermitidis* nov. gen. nov. sp. Spirochaetale de l'intestin de Coloterines praecox. *C R Acad Sci Hebd Seances Acad Sci D* **265:** 1309–1312.

Holt, S.C. (1978) Anatomy and chemistry of spirochetes. *Microbiol Rev* **42:** 114–160.

Hovind-Hougen, K. (1972) Further observations on the ultrastructure of *Treponema pallidum* nichols. *Acta Pathol Scand Sect B* **80:** 297–304.

Hovind-Hougen, K. (1974) The ultrastructure of cultivable treponemes. I. *Treponema phagedenis*, *Treponema vincentii*, and *Treponema refringens*. *Acta Pathol Scand Sect B* **82:** 329–344.

Hovind-Hougen, K. (1976) Determination by means of electron microscopy of morphological criteria of value for classification of some spirochetes, in particular treponemes. *Acta Pathol Scand Sect B* **255:** 1–41.

Hovind-Hougen, K. (1979) *Leptospiraceae*, a new family to include *Leptospira* Noguchi 1917 and *Leptonema* gen nov. *Int J Syst Bacteriol* **29:** 245–251.

Hovind-Hougen, K., and Birch-Andersen, A. (1971) Electron microscopy of the endoflagella and microtubules in *Treponema* Reiter. *Acta Pathol Scand Sect B* **79:** 37–50.

Izard, J., Samsonoff, W.A., Kinoshita, M.B., and Limberger, R.J. (1999) Genetic and structural analysis of the cytoplasmic filaments of wild-type and flagellar filament mutant of *Treponema phagedenis*. *J Bacteriol* **181:** 6739–6746.

Izard, J., Samsonoff, W.A., and Limberger, R.J. (2001) Cytoplasmic filament-deficient mutant of *Treponema denticola* has pleiotropic defects. *J Bacteriol* **183:** 1078–1084.

Jackson, S., and Black, S.H. (1971) Ultrastructure of *Treponema pallidum* Nichols following lysis by physical and chemical methods. I. Envelope, wall, membrane and fibrils. *Arch Mikrobiol* **76:** 308–324.

Jenkins, C., Samudrala, R., Anderson, I., Hedlund, B.P., Petroni, G., Michailova, N., *et al.* (2002) Genes for the cytoskeletal protein tubulin in the bacterial genus *Prosthecobacter*. *Proc Natl Acad Sci USA* **99:** 17049–17054.

Jones, L.J., Carballido-Lopez, R., and Errington, J. (2001) Control of cell shape in bacteria: helical, actin-like filaments in *Bacillus subtilis*. *Cell* **104:** 913–922.

Kremer, J.R., Mastronarde, D.N., and McIntosh, J.R. (1996) Computer visualization of three-dimensional image data using IMOD. *J Struct Biol* **116:** 71–76.

Landis, W.J., Song, M.J., Leith, A., McEwen, L., and McEwen, B.F. (1993) Mineral and organic matrix interaction in normally calcifying tendon visualized in three dimensions by high-voltage electron microscopic tomography and graphic image reconstruction. *J Struct Biol* **110:** 39–54.

Limberger, R.J., and Charon, N.W. (1986) *Treponema phagedenis* has at least two proteins residing together on its periplasmic flagella. *J Bacteriol* **166:** 105–112.

Ma, X., Ehrhardt, D.W., and Margolin, W. (1996) Colocalization of cell division proteins FtsZ and FtsA to cytoskeletal structures in living *Escherichia coli* cells by using green fluorescent protein. *Proc Natl Acad Sci USA* **93:** 12998–13003.

McEwen, B.F., and Marko, M. (1999) Three-dimensional transmission electron microscopy and its application to mitosis research. *Methods Cell Biol* **61:** 81–111.

McEwen, B.F., and Marko, M. (2001) The emergence of electron tomography as an important tool for investigating cellular ultrastructure. *J Histochem Cytochem* **49:** 553–564.

McEwen, B.F., Marko, M., Hsieh, C.-E., and Manella, C.A. (2002) Use of frozen-hydrated axonemes to assess imaging parameters and resolution limits in cryo-electron tomography. *J Struct Biol* **138:** 47–57.

Masuda, K., and Kawata, T. (1989) Isolation and characterization of cytoplasmic fibrils from treponemes. *Microbiol Immunol* **33:** 619–630.

Medalia, O., Weber, I., Frangakis, A.S., Nicastro, D., Gerisch, G., and Baumeister, W. (2002) Macromolecular architecture in eukaryotic cells visualized by cryoelectron tomography. *Science* **298:** 1209–1213.

Moritz, M., Braunfeld, M.B., Guenebaut, V., Heuser, J., and Agard, D.A. (2000) Structure of the gamma-tubulin ring complex: a template for microtubule nucleation. *Nat Cell Biol* **2:** 365–370.

Moter, A., Hoenig, C., Choi, B.K., Riep, B., and Göbel, U.B. (1998) Molecular epidemiology of oral treponemes associ-

ated with periodontal disease. *J Clin Microbiol* **36:** 1399–1403.

O'Toole, E.T., Winey, M., and McIntosh, J.R. (1999) High-voltage electron tomography of spindle pole bodies and early mitotic spindles in the yeast *Saccharomyces cerevisiae*. *Mol Biol Cell* **10:** 2017–2031.

Okada, Y., Wachi, M., Hirata, A., Suzuki, K., Nagai, K., and Matsuhashi, M. (1994) Cytoplasmic axial filaments in *Escherichia coli* cells: possible function in the mechanism of chromosome segregation and cell division. *J Bacteriol* **176:** 917–922.

Okuda, K., Ishihara, K., Nakagawa, T., Hirayama, A., and Inayama, Y. (2001) Detection of *Treponema denticola*. Atherosclerotic Lesions. *J Clin Microbiol* **39:** 1114–1117.

Paster, B.J., Boches, S.K., Galvin, J.L., Ericson, R.E., Lau, C.N., Levanos, V.A., *et al.* (2001) Bacterial diversity in human subgingival plaque. *J Bacteriol* **183:** 3770–3783.

Paster, B.J., Falkler, W.A., Jr Enwonwu, C.O., Indigbe, E.O., Savage, K.O., Levanos, V.A., *et al.* (2002) Prevalent bacterial species and novel phylotypes in avanced noma lesions. *J Clin Microbiol* **40:** 2187–2191.

Riviere, G.R., Riviere, K.H., and Smith, K.S. (2002) Molecular and immunological evidence of oral *Treponema*. the human brain and their association with Alzheimer's disease. *Oral Microbiol Immunol* **17:** 113–118.

Sanchez, M., Valencia, A., Ferrandiz, M.J., Sander, C., and Vicente, M. (1994) Correlation between the structure and biochemical activities of FtsA, an essential cell division protein of the actin family. *EMBO J* **13:** 4919–4925.

Simonson, L.G., Goodman, C.H., Bial, J.J., and Morton, H.E. (1988) Quantitative relationship of *Treponema denticola* to severity of periodontal disease. *Infect Immun* **56:** 726–728.

Swain, R.H., and Anderson, A. (1972) The ultra-structure of species of treponemes and borreliae. In *The Fine Morphology of Spirochaetes*. Babudieri, B, (ed). Rome: Leonardo Edizioni Scientifiche.

Taylor, K.A., Schmitz, H., Reedy, M.C., Goldman, Y.E., Franzini-Armstrong, C., Sasaki, H., *et al.* (1999) Tomographic 3D reconstruction of quick-frozen, Ca^{2+}-activated contracting insect flight muscle. *Cell* **99:** 421–431.

Tchamedeu Kameni, A.P., Couture-Tosi, E., Saint-Girons, I., and Picardeau, M. (2002) Inactivation of the spirochete *recA* gene results in a mutant with low viability and irregular nucleoid morphology. *J Bacteriol* **184:** 452–458.

Thomas, D.D., Navab, M., Haake, D.A., Fogelman, A.M., Miller, J.N., and Lovett, M.A. (1988) *Treponema pallidum* invades intracellular junctions of endothelial cell monolayers. *Proc Natl Acad Sci USA* **8:** 3608–3612.

Wang, X., Huang, J., Mukherjee, A., Cao, C., and Lutkenhaus, J. (1997) Analysis of the interaction of FtsZ with itself, GTP, and FtsA. *J Bacteriol* **179:** 5551–5559.

Wicher, K., Wicher, V., Abbruscato, F., and Baughn, R.E. (2000) *Treponema pallidum* subsp. pertenue displays pathogenic properties different from those of *T. pallidum* subsp. pallidum. *Infect Immun* **68:** 3219–3225.

Wiegand, S.E., Strobel, P.L., and Glassman, L.H. (1972) Electron microscopic anatomy of pathogenic *Treponema pallidum*. *J Invest Dermatol* **58:** 186–204.

Woltsche-Kahr, I., Schmidt, B., Aberer, W., and Aberer, E. (1999) Pinta in Austria (or Cuba?): import of an extinct disease? *Arch Dermatol* **135:** 685–688.

You, Y., Elmore, S., Colton, L.L., Mackenzie, C., Stoops, J.K., Weinstock, G.M., and Norris, S.J. (1996) Characterization of the cytoplasmic filament protein gene (*cfpA*) of *Treponema pallidum* subsp. *pallidum*. *J Bacteriol* **178:** 3177–3187.

Zemper, E.D., and Black, S.H. (1978) Morphology of freeze-etched *Treponema refringens* (Nichols). *Arch Microbiol* **117:** 227–238.